Structure, dielectric, and temperature-dependent conductivity studies of the Li_2FeSiO_4/C nano cathode material for lithium-ion batteries

P. Sivaraj, K. P. Abhilash, B. Nalini, P. Balraju, Sudheer Kumar Yadav, S. Jayapandi & P. Christopher Selvin

Ionics
International Journal of Ionics The Science and Technology of Ionic Motion

ISSN 0947-7047

Ionics
DOI 10.1007/s11581-018-2685-1

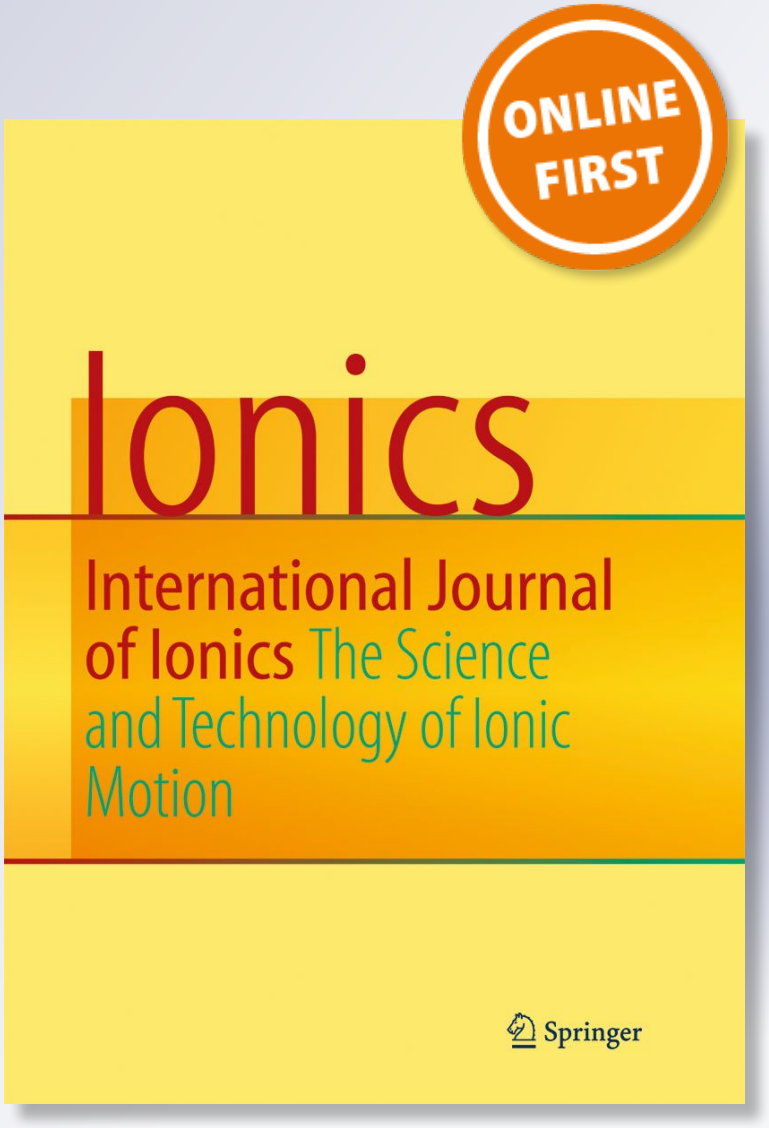

Springer

Ionics
https://doi.org/10.1007/s11581-018-2685-1

ORIGINAL PAPER

Structure, dielectric, and temperature-dependent conductivity studies of the Li_2FeSiO_4/C nano cathode material for lithium-ion batteries

P. Sivaraj[1,2] · K. P. Abhilash[3,4] · B. Nalini[5] · P. Balraju[6] · Sudheer Kumar Yadav[4] · S. Jayapandi[7] · P. Christopher Selvin[2]

Received: 19 April 2018 / Revised: 5 August 2018 / Accepted: 7 August 2018

Abstract

The electrical conductivity plays a vital role in the enhancement of the electrochemical performance of Li_2FeSiO_4 type systems. In most of the system, the elevated temperature operation creates severe structural re-orientation, which cause thermal runway in LIBs. Hence, the exploration of the impacts of temperature on the electrical properties of Li_2FeSiO_4 nano cathode can emphasize to optimize the operating temperature for the LIBs. The lithium-ion diffusion kinetics on the Li_2FeSiO_4/C at different temperatures (− 5 to 400 °C) has been investigated. Rietveld refinement of the XRD data ensured that the Li_2FeSiO_4/C possess an orthorhombic structure with $Pmn2_1$ space group. The FE-SEM and TEM micrographs display the spherical morphology of the nanoparticles with an average particle size of 25 nm. The single-phase formation and presence of carbon have been elucidated by FTIR, Raman, and XPS analysis. The Li_2FeSiO_4/C exhibits an excellent electrical conductivity of 1.022×10^{-4} Scm^{-1} at room temperature. The electrochemical reversibility of the Li_2FeSiO_4/C cathode in an aqueous electrolyte has been explored by cyclic voltammetry (CV) analysis. The Li_2FeSiO_4/C nano cathode exhibits excellent electrical properties at the elevated temperatures (from 50 to 125 °C) which can be optimized to perform stable operation of the all solid-state lithium-ion batteries.

Keywords Cathode material · Electrical properties · Lithium-ion batteries

Introduction

The researchers are being searched for sound cathode materials to meet the requirement of large-scale storage application such as hybrid electric vehicles and devices coupled with wind and solar energy. The transition metal oxides $LiMO_2$ (M = Co, Ni, and Mn), spinel compounds ($LiMn_2O_4$), and olivine compounds ($LiMPO_4$ (M = Fe, Ni, Co, and Mn)) are the existing promising cathode materials for lithium-ion batteries [1]. These conventional materials have several limitations such as high toxicity, expensive, low theoretical capacity, etc. [1]. Several efforts have been attempted to find an alternative cathode material with high capacity, inexpensive, nontoxic, thermally stable, and safe operation for hybrid electric vehicles [2].

Recently, the transition metal orthosilicates(Li_2MSiO_4, M = Fe, Mn, Co, Ni, etc.,) are being searched as a high capacity alternative cathode material for advanced high energy density lithium-ion batteries [3]. Among these, the Li_2FeSiO_4 has attracted great interest within battery community due to its remarkable features such as higher theoretical capacity 332 $mAhg^{-1}$, two Li-ion extraction per formula unit, high safety, and operation over wide range of temperature [3–5]. In addition to this, the Li_2FeSiO_4 is a green material in which the iron (Fe) and silica (Si) are earth-abundant elements, nontoxic, and inexpensive. The Li-Fe-Si-O bonds are very strong

✉ P. Christopher Selvin
csphysics@buc.edu.in; pcsphyngmc@rediffmail.com

1 Materials Research Centre, Department of Physics, N.G.M.College, Pollachi, Coimbatore 642001, India

2 Solid State Ionics and Luminescence Laboratory, Department of Physics, Bharathiar University, Coimbatore 641046, India

3 Department of Physics, National University of Singapore, Singapore 117542, Singapore

4 Herbert Gleiter Institute of Nanoscience, Nanjing University of Science and Technology, Nanjing 210094, China

5 Department of Physics, Avinashilingam Institute for Home Science and Higher Education for Women, Coimbatore 641043, India

6 Department of Physics, Coimbatore Institute of Technology, Coimbatore 641014, India

7 School of Physics, Madurai Kamaraj University, Madurai 625021, India

Published online: 18 August 2018

which hinder the oxygen migration at elevated temperatures and to prevent the thermal runaway. In spite of these advantages, Li_2FeSiO_4 suffers very low intrinsic electronic/ionic conductivity (10^{-12} Scm^{-1}) and slow lithium diffusion mobility which hinder the electrochemical performance, thus limiting the application to the market potential [6]. Numerous strategies have been employed to address these primary challenges by carbon coating, downsizing the particle and metal transition ions doping [7–10].

Even though the strategies have improved the structure, electrical properties, and electrochemistry of the Li_2FeSiO_4, still it is far from the market demands. Several researchers have studied the electrochemical performance of Li_2FeSiO_4 cathode material and reported its severe capacity fading. The capacity fading of the sample mainly depends on the structural instability, cycling rate, operation temperature, etc.; among these factors, the operation temperature plays a vital role in achieving best battery performance. The safe operation at elevated temperature is one of the major challenges reported by several researchers [11]. The temperature has significant impacts on the performance, safety, and cycle life of LIBs especially when it finds its application toward the HEVs. The temperature variations, especially at high temperatures, can cause a thermal runway which ignites fire and explosion [11, 12]. The impact of temperature on battery performance of various cathode materials such as $LiCoO_2$, $LiMnO_2$, $LiCoO_2$/graphite, $LiFePO_4$ etc. have been explored [13–15]. However, the dependence of temperature on the electrical properties of the Li_2FeSiO_4 cathode has not yet been elucidated, so far. Most of the historical reports [12] demonstrate that the volume expansion and phase transition are the major factors affecting the battery performance.

The recent studies [16] had reported that the Li_2FeSiO_4 cathode exhibits severe capacity fading after first cycle has attributed to the severe volume expansion but it fails to examine the contribution of temperature on unit cell volume expansion and electrical performance of the material. The Li_2FeSiO_4/C is highly sensitive to the temperature and exhibits high capacity at 100 °C which have been elucidated by Rui tana et al. [17]. The study revealed that the enhanced performance is due to the high-temperature-dependent diffusivity and electronic conductivity, which clearly establish that the temperature variations play a vital role in the electrochemical performance of Li_2FeSiO_4. The battery performance not only depends on the high temperature but also influenced by low temperature, hence the low-temperature-dependent electrical study is also immense important for operating the battery at low-temperature range. The operating temperature plays the key role to design thermally stable high-performance LIBs which demands the investigation on the electrical and electrochemical performance of Li_2FeSiO_4/C at different temperatures. Hence, the exploration of the dependence of temperature on the electrical conductivity is immensely important for optimizing the operation temperature of LIBs.

The poor electrical performance at elevated temperature is one of the inherent problems in the Li_2FeSiO_4 cathode. Very recently, the temperature-dependent (− 40 to 120 °C) electrical conductivity of the Li_2FeSiO_4 without carbon has been studied by Lei Liu et al. [18] and reported that the ionic conductivity and electronic conductivity of the non-carbon-coated sample are 1.32×10^{-8} S/cm and 2.8×10^{-8} S/cm, respectively at room temperature. The pure Li_2FeSiO_4 material possessed very lower electronic/ionic conductivity but the electrical properties play crucial role in achieving the high performance of a battery [3]. Hence, in the present work, the temperature-dependent electrical conductivity of the Li_2FeSiO_4 coated by carbon cathode has been explored from low temperature (− 5) to high temperature up to 400 °C. According to the literature, the LFS/C with orthorhombic structure ($Pmn2_1$) displays excellent electrochemical stability than that of all other polymorph structure (Pmna, $P2_1/n$, $Pna2_1$, etc.) [19]. In this work, we have directly prepared electrochemically stable orthorhombic structure ($Pmn2_1$) of Li_2FeSiO_4/C cathode and investigated its temperature-dependent electrical conductivity for the first time. The present work thoroughly investigated the influence of temperature on electrical performance of the Li_2FeSiO_4/C ($Pmn2_1$) cathode from low temperature (− 5 °C) to higher temperature (400 °C) for the first time, which has not been elucidated so far, which is important in order to obtain best performance of LFS/C-based all solid-state lithium-ion batteries. The present work also includes studying the temperature dependence of dielectric and modulus analysis of Li_2FeSiO_4/C cathode which provides a clear lithium-ion transport mechanism and conductivity relaxation process in the material. In addition to that, the electrochemical behavior of the Li_2FeSiO_4/C cathode has been examined at room temperature in order to explore the electrochemical reversibility and cycling stability.

Materials and methods

The Li_2FeSiO_4/C nano cathode material was prepared by the modified sol-gel method, reported in our previous work [20]. The lithium acetate (Sigma Aldrich, regent grade 99.55%), iron nitrate nonahydrate (Sigma Aldrich, 99.9%), TEOS (Sigma Aldrich 99.995), and citric acid were used as raw material for the preparation of the Li_2FeSiO_4 by sol-gel method. In this work, a slight modification in the synthesis process of Li_2FeSiO_4/C was attempted. The 0.2 mol lithium acetate and 0.1 mol iron nitrate nonahydrate were dissolved in 50 ml distilled water and stirred well by the magnetic stirrer. The stoichiometric amounts of TEOS were dissolved in 20 ml

ethanol and stirred well. Then the solution mixed with water solution and saturated aqueous solution of 0.1 mol of citric acid was added drop by drop. The precursor solution was heated at 80 °C under magnetic stirring till getting the gel-like low viscous solution. The gel solution was heated at 85 °C for 24 h in an incubator oven for solvent evaporation. The resultant product is further calcined at 700 °C in a tubular furnace under Ar atmosphere over 10 h, resulting in the grayish black Li_2FeSiO_4/C nanopowder.

The structural characterization was carried out by powder XRD (XRD-Shimadzu-6000) analysis. The morphology of the prepared samples was analyzed by Carl Zeiss Sigma field emission scanning electron microscope (FE-SEM). The optical study of the sample was analyzed by the FTIR (Shimadzu 220-93270-55 IRTracer-100). The Raman spectra were analyzed over the range of 200–3000 cm^{-1} by a Raman microspectroscopy (RM-1000 Renishaw confocal) with 514 nm laser radiation at a laser power of 0.042 mW. The X-ray photoelectron spectroscopy spectra characterization has been carried out using SPECS XR50 instrument. The XPS was recorded using Al Kα (Hμ = 1486.6 eV) radiations and the sample has been investigated in an ultra high vacuum of 10^{-10} mbar. The thermal analysis (TG-DTA) of the as prepared LFS/C was recorded by simultaneous thermogravimetry/differential thermal analyzer (DTA-60AH). The thermal measurement was employed between room temperature to 700 °C at a heating rate of 10 °C/min under N_2 atmosphere. The Li_2FeSiO_4/C pellet was prepared by applying a pressure around 3 tons to form a 1.4-mm thickness and 12-mm diameter. The pellet was prepared at room temperature; there was a possibility to form small amount of carbon-related impurity phases on the surface of the Li_2FeSiO_4/C due to its exposure to air. Hence, the pellet was sintered at 400 °C for 2 h under argon atmosphere in order to remove the impurity compounds on the surface of the sample. The electrical conductivity of the sample was carried out by complex impedance spectrometer (HIOKI LCR 3532-50; frequency range: 42 Hz to 5 MHz) using silver paste as contact electrodes on either side. The low-temperature conductivity of the sample was carried out by putting the sample containing liquid nitrogen system and the measurement is carried out from lower to higher temperatures (− 5 to 400 °C).

Electrochemical characterization

The electrochemical behavior of the Li_2FeSiO_4 cathode was examined by cyclic voltammetry using three electrodes in an aqueous system. The electrode was prepared using a slurry comprised of 85% active material, 10% acetylene black (conductive carbon), and 5% PVdF binder. The mixer was stirred with *N*-methyl-2-pyrrolidone solution, and the viscous slurry was coated onto aluminum foil by doctor blade method and subsequently dried at 100 °C for 10 h to ensure complete solvent removal. In the present work, the electrochemical system (Biologic, SP 150) with three electrodes set up has opted for cyclic voltammetry analysis. Apart from the working electrode (material under investigation), the saturated calomel and platinum were preferred as the reference and counter electrodes, respectively. The 5 M aqueous $LiNO_3$ served as the electrolyte solution. The redox activity of the Li_2FeSiO_4 has been investigated for various scan rates ranging from 10 to 100 mV/s at an appropriate potential window of the water solvent (< 1.25 V) at room temperature.

Results and discussion

Structural analysis

Figure 1 shows the XRD pattern of Li_2FeSiO_4/C cathode material. The sharp intense diffraction peaks observed at 2θ = 16.17°, 24.46°, 28.12°, 33.4°, 35.77°, 39.01°, 50.10°, and 60.23° are indexed to the crystalline peaks of the orthorhombic structure of Li_2FeSiO_4/C cathode. The XRD peaks of Li_2FeSiO_4/C can be assigned to an orthorhombic structure with $Pmn2_1$ space group. The prepared sample is absent of any kind of impurities such as Fe_3O_4, $LiCO_3$, Li_2SiO_3, which indicate the formation of single-phase Li_2FeSiO_4/C material. The Rietveld refinement (GSAS + EXPGUI) has been carried out multiple times and the exact lattice parameters are tabulated in Table 1. The reliability factors are found to be $R_W p$ = 7.4%, s = 1.27 and the refined structure parameters are a = 6.28 Å, b = 5.33 Å, c = 4.97 Å, and $\alpha = \gamma = \beta = 90$ for Li_2FeSiO_4/C orthorhombic ($Pmn2_1$) phase which are consistent with the reported values in the previous literatures [21, 22]. The refinement results are ensured that the prepared sample possess an orthorhombic structure with a space group of $Pmn2_1$. The crystallite size of the Li_2FeSiO_4/C is calculated

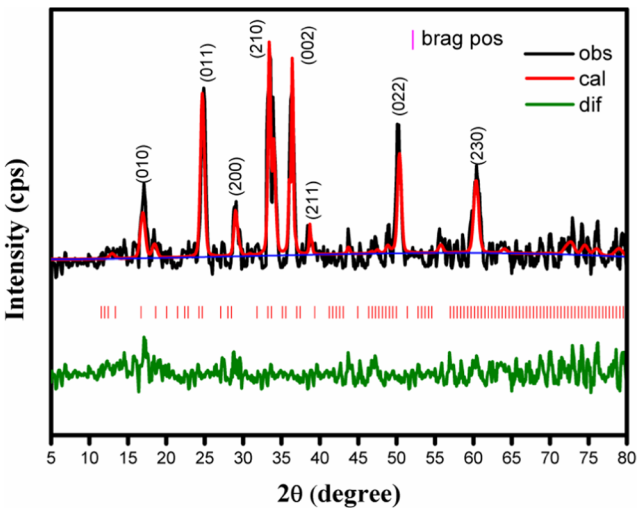

Fig. 1 The Retveld refined XRD pattern of the Li_2FeSiO_4/C cathode material

Table 1 The final results of the Rietveld refinement for the Li_2FeSiO_4/C material

Lattice parameters	$a = 6.28$ Å
	$b = 5.33$ Å
	$c = 4.97$ Å
	$\beta = 90.13°$
Cell volume (Å^3)	166.35(7)
Mean crystallite size (nm)	19(3)
R_{wp} (factor)	7.43

using Debye-Scherrer's formula, and is found to be 19 nm. There is no crystalline carbon that can be obviously detected in the XRD pattern, revealing that the formed carbon layer is probably in the amorphous phase due to its low content or low graphitization degree [23].

Vibrational analysis (FTIR and Raman)

The FTIR spectrum of the prepared Li_2FeSiO_4/C sample is shown in Fig. 2a. The characteristic vibrational band of Li_2FeSiO_4/C observed at 901 cm^{-1} is attributed to the stretching vibration of Si-O bonds in $(SiO_4)^{4-}$ tetrahedras [23]. The modes at 525, 576 cm^{-1} are due to the bending vibration of $(SiO_4)^{4-}$ [23, 24]. The absorption peaks at 420, 444, and 494 cm^{-1} can be assigned to the possible Li-O stretching modes in LiO_4 tetrahedra [25]. The vibrational peaks at 1440 and 1485 cm^{-1} are assigned to the characteristic peaks of carbonate (e.g., Li_2CO_3) and have formed on the surface of Li_2FeSiO_4/C due to its exposure to air. The Li_2CO_3 phase is not detectable by X-ray diffraction due to its low content and crystallinity [26]. The peak noticed at 1594 cm^{-1} can be contributed to the stretching vibration of a C=C double bond resulting from carbon layer [26].

The carbon coating layer on the particle surface of the Li_2FeSiO_4/C cathode materials has been evaluated by Raman spectroscopy, shown in Fig. 2b. In the Raman spectra, two intense broad bands have been originated in 1345 and 1594 cm^{-1}. The Raman signal at 1345 cm^{-1} is due to the D (disordered) line which is associated with disordered allowed zone-edge modes of graphite (sp^2) [27]. The band located at 1594 cm^{-1} is attributed to the G (Graphite) line which is associated with allowed E_2g zone center mode of crystalline graphite [28]. The calculated integrated Raman intensity ratios of I_D/I_G band for the Li_2FeSiO_4/C is found to be 0.87, the lower I_D/I_G ratios is an indication of the presence of a larger amount of sp^2-type graphene carbon coated in the sample [29]. It is noted that the electronic conductivity of the Li_2FeSiO_4 cathode mainly depends on the structure of carbon coating [29]. In addition to this, a comparatively smaller signal observed at 460 cm^{-1} is due to the characteristic Raman vibrations of SiO_4 functional group in the Li_2FeSiO_4/C cathode.

XPS analysis

The XPS spectrum of as prepared Li_2FeSiO_4/C cathode is shown in Fig. 3. The XPS spectrum ensured the presence of Si, O, Fe, C, and Li in the sample. The C1s peak of the Li_2FeSiO_4/C can be resolved in to three components centered at 284.3, 287, and 291 eV attributed to C-C, C=O, and CO_3^{2-} bonds, The peaks clearly verifies the presence of carbon in the prepared sample. The origination of CO_3^{2-} groups occurs from the residual carbon on the Li_2FeSiO_4/C surface, which forms small amount of Li_2CO_3 on the particle surface due to its exposure to air [26]. However, the absence of peaks corresponding to the Li_2CO_3 in the XRD spectra clearly verifies that it forms only in traces amount, which appears in the more sensitive XPS measurements. The carbon content of 11.13% (At%) has been estimated by the peak area calculation using the CASA XPS Software for the prepared sample (Fig. 3). The Fe2p spectrum consists of two components, the peak originated at binding energy 710.6 eV can be assigned to the Fe^{2+} in

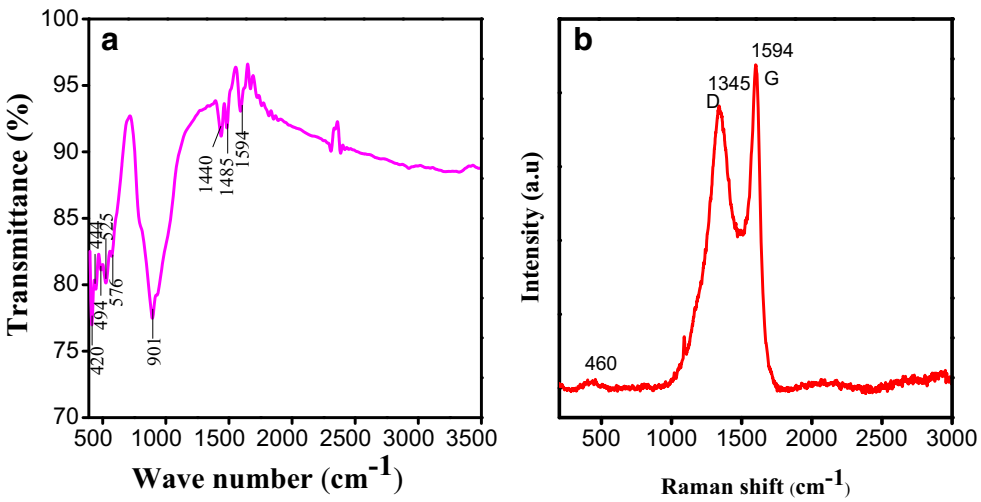

Fig. 2 **a** FTIR spectra and **b** Raman spectra of the Li_2FeSiO_4/C cathode material

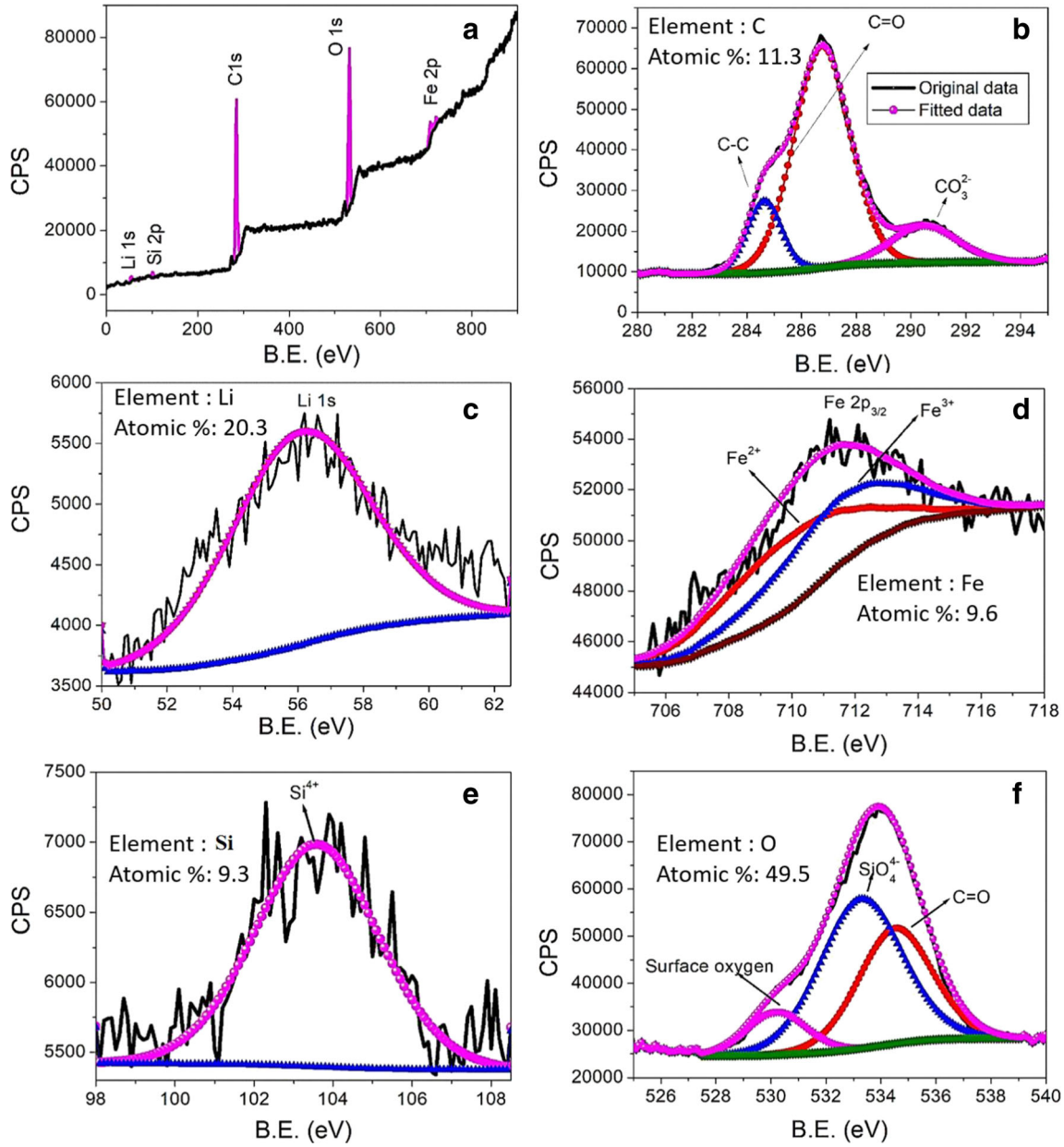

Fig. 3 The XPS spectra of the as prepared Li_2FeSiO_4/C cathode material

Li_2FeSiO_4/C [30], and the peak at higher binding energy of 712.4 eV is due to the Fe^{3+} in Li_2FeSiO_4/C. The presence of Fe^{3+} in the Li_2FeSiO_4/C originates due to the unavoidable air exposure during the XPS measurement [26]. The Li 1s spectrum shows a single broad peak at 56.4 eV, which confirms the presence of Li in the prepared sample. The O 1s spectra of the as prepared Li_2FeSiO_4/C can be resolved into four components centered at 530.6 and 532.4, which originates from the surface oxygen in Li_2FeSiO_4 and silica-oxygen tetrahedron (SiO_4^{4-}). The peaks at higher binding energy (534 and 534.8 eV) originate from some carboxyl compounds (i.e., Li_2CO_3) [31]. It should be specially noted that the Si 2p spectrum displays a peak at 103.2 eV that originates from Si^{4+} in Si-O tetrahedron which clearly represents the formation of the orthosilicate structure SiO_4^{4-} of the Li_2SiO_4 [32]. The existence of the pure Li_2FeSiO_4 phase has been confirmed by Fe2p, Li1s, O1s, and Si2p peaks that occurs in the in XPS spectra.

TG-DTA analysis

The thermogram of the Li_2FeSiO_4/C which exhibits three different thermal event is shown in Fig. 4a. The events start at 50 °C and it shows a gradual weight loss (10.12%) up to 150 °C, which is attributed to the decomposition of water and ethanol solvent evaporation from the starting materials. The result revealed that the sample has been preserved by annealing above 150 °C then it

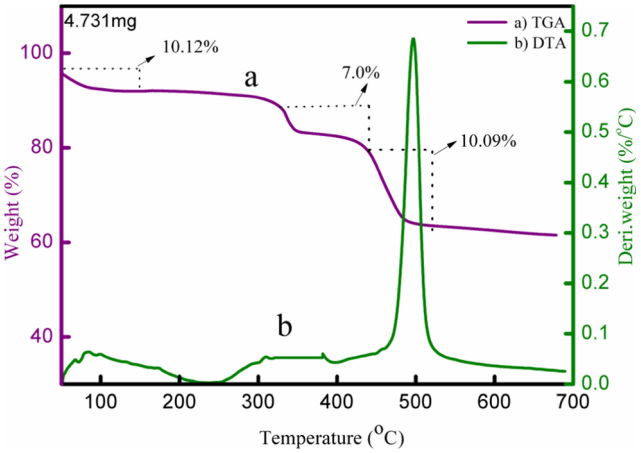

Fig. 4 The DTA analysis of the Li_2FeSiO_4/C cathode material

has been allowed to explore the structural and electrical properties. A small weight loss (7%) occurred in the sample at 300–415 °C is due to the decomposition of the citric acid (gelating agent and carbon source). The third thermal event with sharp endotherm (10.09% weight loss) at 410–498.23 °C can be assigned to parent reaction occurring and carbonization of the citric acid [16]. By TG analysis, the estimated carbon content for the Li_2FeSiO_4/C material is 10.09%. The differential thermal analysis (DTA) has been used to evaluate the possible reaction occurring during the synthesis of Li_2FeSiO_4/C nano cathode material. Figure 4b shows the DTA of the sample, in which a sharp exothermic peak observed at 500 °C indicates the crystallization process, which is completed by 550 °C. In our previous report, the calcination temperature has been optimized as 700 °C to prepare single-phase Li_2FeSiO_4/C nano cathode material without impurity [20]. Hence, the calcination temperature of the present work has been chosen as 700 °C to obtain a single-phase orthorhombic structure with $Pmn2_1$ space group.

Morphological analysis

Figure 5a shows the FE-SEM micrograph of the Li_2FeSiO_4/C cathode material. It is noticed that the nanosphere particles are homogeneously distributed on the skin area of the sample with average particle ranges from 25 to 38 nm. The particle size obtained from the micrograph is larger than the crystallite size (19 nm, from XRD pattern) which indicates that the sample

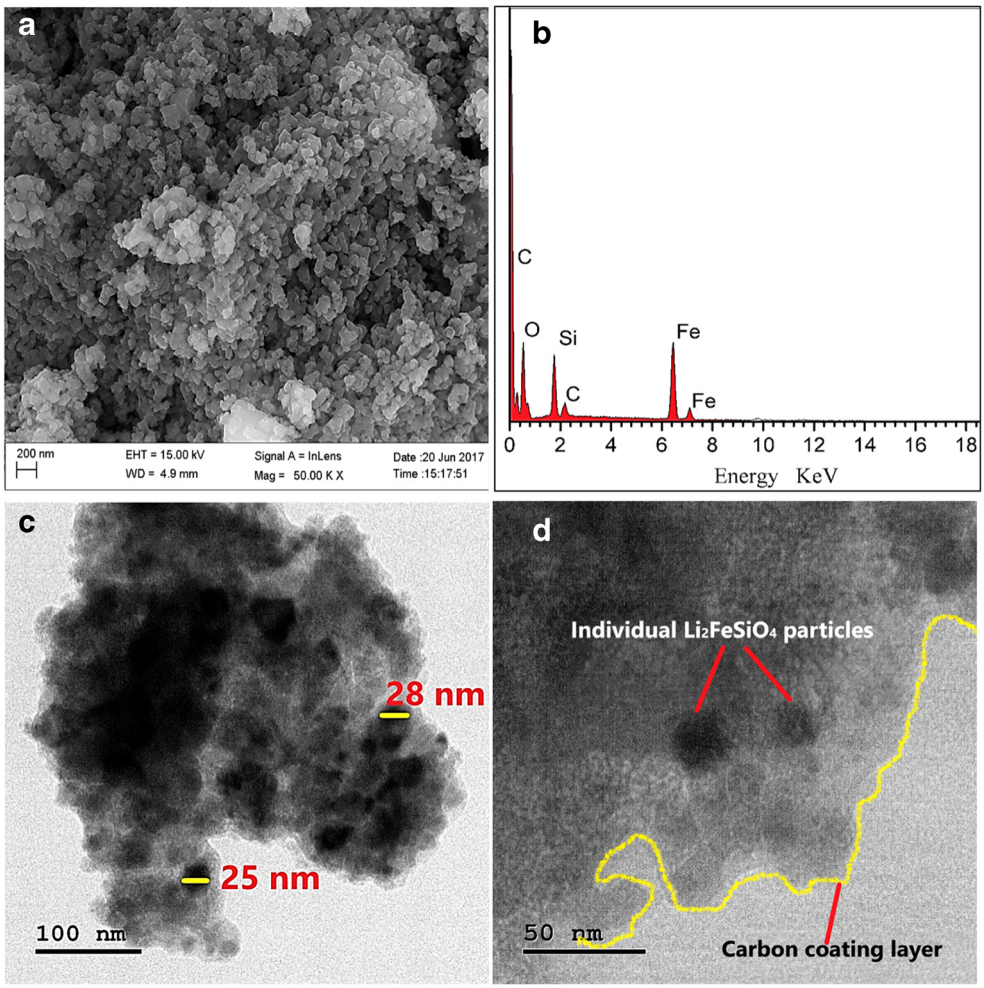

Fig. 5 **a** FE-SEM micrograph, **b** EDAX spectra, and **c**, **d** TEM image of the Li_2FeSiO_4/C cathode material

possessed polycrystalline nature. In addition to that, the small primary nanosphere particles are aggregated with each other to form Li_2FeSiO_4/C secondary particles. The nanosphere particles are increasing the tap density of the cathode material; the larger sphere particles provide the denser packing while the smaller size of the primary nanoparticles significantly enhances the Li-ion and electron conduction [8]. The better morphology of the sample is obtained which reflects in all the properties of the Li_2FeSiO_4/C material. The TEM analysis has been carried out for the prepared sample which ensured that the prepared samples possessed the nanoparticles with average size ranges from 25 to 30 nm (Fig. 5c). The carbon coating has been ensured by TEM analysis (Fig. 5d). The EDS spectrum (Fig. 5b) confirms the presence of the expected elements in the sample.

The temperature-dependent conductivity studies

The AC impedance analysis has been used to investigate the charge transport process in grain and grain boundaries of the materials for a wide frequency range (42 Hz to 5Mz) at different temperatures (− 5 to 400 °C). Figure 6a(a–h) shows the Nyquist plot of Li_2FeSiO_4/C cathode material at low temperatures (− 5 to 50 °C). The conductivity at lower temperatures has been carried out by putting the sample containing the liquid nitrogen and taking the conductivity from the lowest to higher. All the plots were fitted with Z-view software and the equivalent circuit is provided. In all the plots, the solid line represents fitted data and the dot lines are the experimental data. The plots show the combined high-frequency semicircle and low-frequency semicircle indicating that the grain and grain boundary contributed to the impedance behavior of the sample for all the low temperatures. The obtained plot has been resolved using the Z-view software by employing the equivalent circuit as shown in Fig. 6(a, b). This one parallel resistance (R)-constant phase element (CPE) combination represents one semicircle. The diameter of the semicircles has been decreased with increase in the temperature. The Li_2FeSiO_4/C material does not exhibit a perfect semicircle at the low-temperature range between − 5 and 20 °C shown in Fig. 6a(a–f), which causes the poor electrical performance at low temperatures. The depressed semicircle at high frequency is attributed to the bulk properties [33] of the Li_2FeSiO_4/C cathode material and a spike is due to the electrode polarization. The low-temperature behavior of the sample can be referred to Non-Deby type of relaxation which depends on several factors such as grain size, grain boundary, atomic defects distribution, and volume expansion. The Non-Deby nature of the conductivity can be clearly verified from the depressed semicircle with its center lies below the *Z*' axis (while the perfect semicircle with the center point lies in the frequency axis represents the Deby nature of the sample) that obtained for the present samples [34–36]. Figure 6b(a–l) shows the Nyquist plots of the sample at the temperature range between 75 and 400 °C. In the intermediate temperature range (50 to 125 °C), the Li_2FeSiO_4/C cathode shows high-frequency semicircle and low-frequency semicircle with spike indicating the resolved grain (bulk) and grain boundary effect. From the capacitance value, the grain and grain boundary component of the resistance can be resolved from the single semicircle that was obtained for the sample [37]. A combined semicircle with resolving the grain and grain boundary components have been obtained for the lower temperatures and at high temperatures (250 to 400 °C) range. It demonstrates that the electrical performance of the Li_2FeSiO_4/C material depends on the temperature. The depression of the semicircles is the clear indication of the polarization phenomenon that occurs in the sample. For the polycrystalline Li_2FeSiO_4/C material, impedance

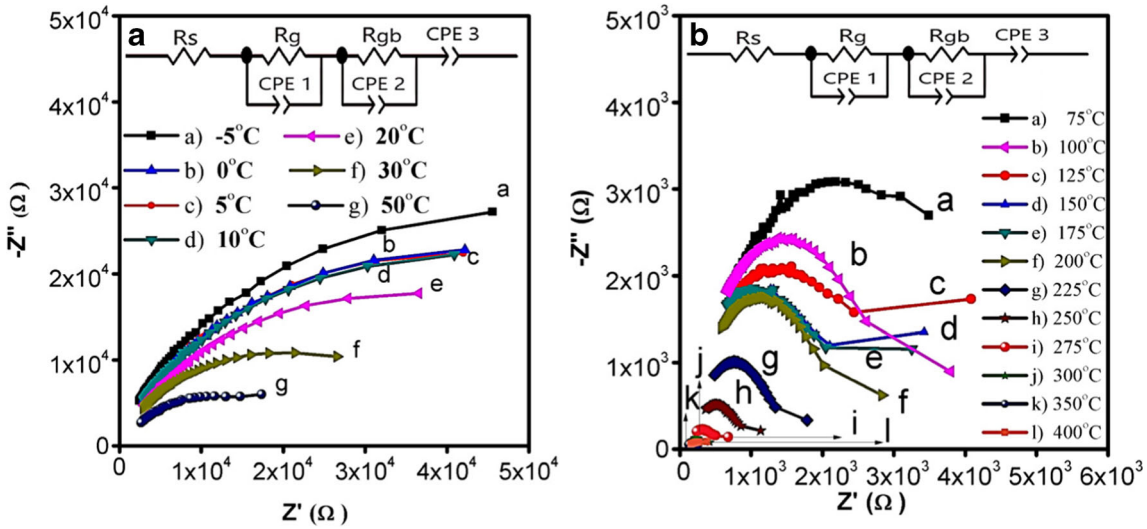

Fig. 6 **a**, **b** Nyquist plot of Li_2FeSiO_4/C cathode material at different temperatures (− 5 to 400 °C)

measurement at intermediate temperature (50 to 125 °C) can raise the grain and grain boundary effects which are consistent with the brick-layer model [38].

The grain and grain boundary conductivity of the materials are calculated using the following equations:

$$\sigma_g = d/R_gA$$
$$\sigma_{gb} = d/R_{gb}A$$

where d is the thickness of the pellet(1.4 mm), A is the area of the samples (0.2825cm^2), R_{gb} is the grain boundary resistance, R_g is the grain resistance, σ_g is the grain (bulk) conductivity Scm^{-1}, and σ_{gb} is the grain boundary conductivity of the samples respectively. The R_g and R_{gb} are obtained from Nyquist plots using Z-view software with equivalent circuit models. The room temperature grain and grain boundary conductivity of the Li_2FeSiO_4/C sample is found to be 1.007×10^{-4} Scm^{-1} and 2.300×10^{-5} Scm^{-1}. The obtained room temperature conductivity of the Li_2FeSiO_4/C is far better than the reported value (~10^{-12} Scm^{-1}) in the literature [5, 39]. The calculated electrical conductivity of sample at different temperatures is listed in Table 2. From Table 2, the sample shows a disordered conductivity for particular temperature (150 to 200 °C). At this temperature, the samples are exhibited almost similar electrical conductivity. This disordered conductivity of the Li_2FeSiO_4/C might be attributed to structural reorientation occuring in the sample. The conductivity increases with increase in the temperature and due to the hoping mechanism of thermally activated charge carriers [40]. None of the researchers has reported the temperature dependence of the conductivity of Li_2FeSiO_4/C material. However, several researchers reported that the influences of temperature $LiFePO_4$ (similar compound of Li_2FeSiO_4) which demonstrated that the material exhibits phase change in the range of 423 to 473 k [41]. The study reported that the phase change gives no signature peak in DSC curve but originates from coexistence of mixed phases in the sample [42, 43]. This can be correlated with high-temperature non semicircle nature that occurs in the sample. At 400 °C, the Nyquist plot does not show a regular behavior which ensured that the intermediate phase transitions have a key role in the anomalously high-temperature electrical performance of the orthosilicate Li_2FeSiO_4/C sample. The Li_2FeSiO_4/C material is very sensitive to the temperature dependence of the electrical conductance reported by Rui Tana et al. [17] and the study revealed that the Li_2FeSiO_4/C exhibits high rate and capacity at 100 °C. Hence, the present exploration of the dependence of temperature on electrical conductivity is highly useful to design thermally stable high-performance all solid-state LIBs.

Figure 7a, b shows the real (Z') part of impedance as the function of frequency at different temperatures in the Li_2FeSiO_4/C material. It is noted that the Z' value decreases with increasing temperature at low frequency. In addition to that, the

Table 2 The calculated grain and grain boundary conductivity of the Li_2FeSiO_4/C material at different temperatures (− 5 to 400 °C)

Temperature (°C)	Grain R_g (Ω)	Grain boundary R_{gb} (Ω)	CPE1 (F) $\times 10^{-12}$	CPE2(F) $\times 10^{-9}$	CPE2(F) $\times 10^{-9}$	Grain conductivity (Scm^{-1})	Grain boundary conductivity (Scm^{-1})	Total conductivity (Scm^{-1})
− 5	7562	80,536	0.23	6.12	4.45	5.615×10^{-5}	5.272×10^{-6}	6.142×10^{-5}
0	6223	77,563	0.89	7.32	4.48	6.823×10^{-5}	5.474×10^{-6}	7.371×10^{-5}
5	6089	55,345	1.23	7.01	5.09	6.973×10^{-5}	7.672×10^{-6}	7.740×10^{-5}
10	5864	47,456	0.89	7.89	5.87	7.241×10^{-5}	8.947×10^{-6}	8.136×10^{-5}
15	5434	46,675	1.50	7.92	3.45	7.814×10^{-5}	9.097×10^{-6}	8.724×10^{-5}
20	5062	43,451	1.45	8.01	4.90	8.388×10^{-5}	9.772×10^{-6}	9.365×10^{-5}
30	4243	32,898	0.46	8.12	5.07	8.934×10^{-5}	1.290×10^{-5}	1.022×10^{-4}
50	3278	16,284	1.13	9.23	6.12	1.295×10^{-4}	2.607×10^{-5}	1.556×10^{-4}
75	2879	15,777	1.11	10.45	7.45	1.474×10^{-4}	2.691×10^{-5}	1.744×10^{-4}
100	2175	7345	1.08	10.78	7.09	1.951×10^{-4}	5.781×10^{-5}	2.530×10^{-4}
125	1515	6375	1.23	11.30	8.91	2.802×10^{-4}	6.660×10^{-5}	3.468×10^{-4}
150	926	6152	1.28	12.23	9.32	4.585×10^{-4}	6.902×10^{-5}	5.275×10^{-4}
175	845	5702	1.48	14.34	10.34	5.863×10^{-4}	7.447×10^{-5}	6.610×10^{-4}
200	873	5235	1.67	12.34	11.65	5.673×10^{-4}	8.111×10^{-5}	6.495×10^{-4}
225	334	4879	1.73	13.98	12.45	1.271×10^{-3}	8.703×10^{-5}	1.358×10^{-3}
250	311	3023	1.69	15.15	17.56	1.365×10^{-3}	1.404×10^{-4}	1.505×10^{-3}
275	259	1578	1.77	16.18	19.56	1.639×10^{-3}	2.690×10^{-4}	1.908×10^{-3}
300	245	1192	2.11	17.23	20.34	1.733×10^{-3}	3.563×10^{-4}	2.089×10^{-3}
400	196	879	2.13	18.78	21.34	1.851×10^{-3}	4.830×10^{-4}	2.335×10^{-3}

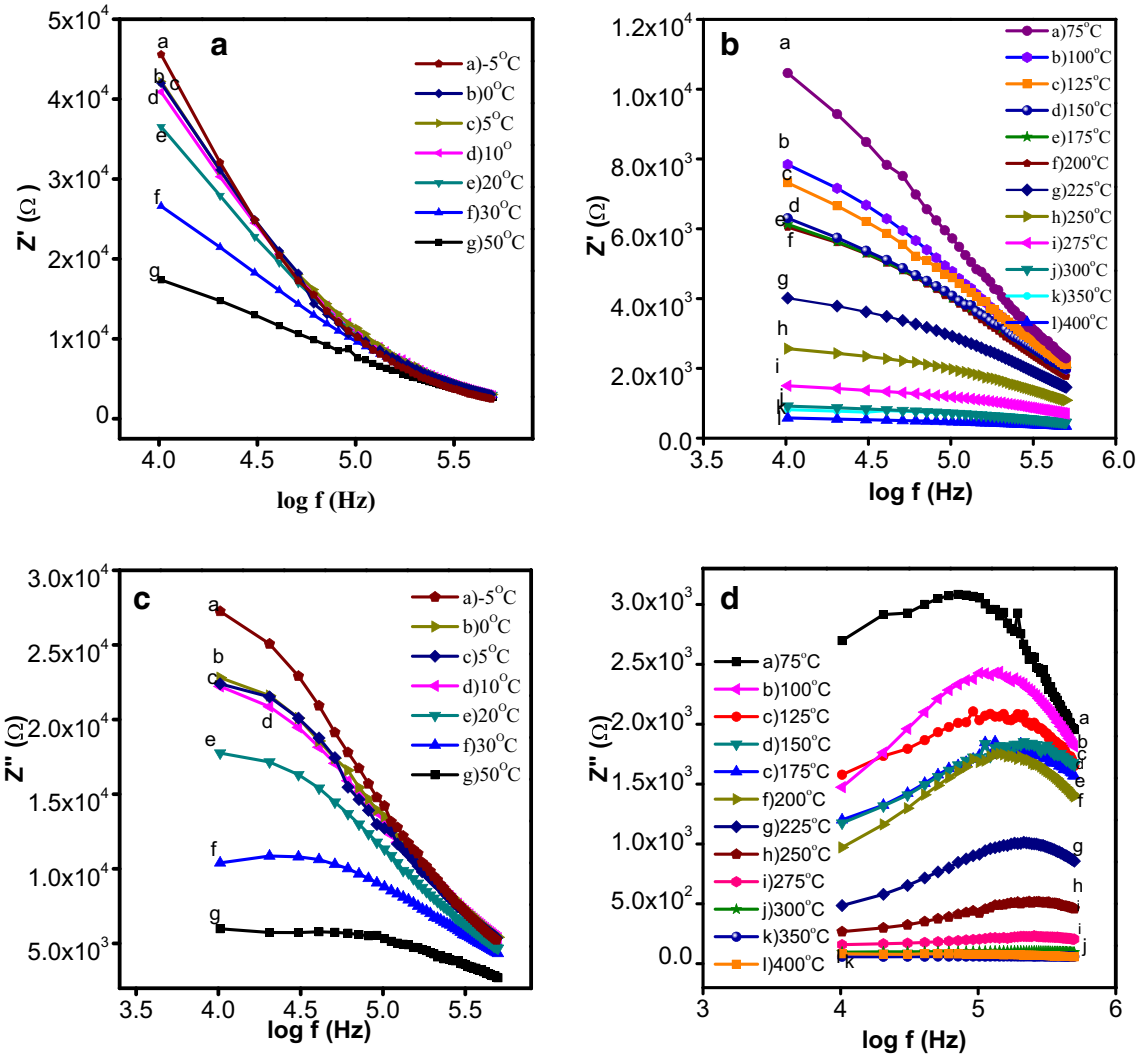

Fig. 7 **a**, **b** Real part (Z') of impedance as a function of frequency and **c**, **d** imaginary part (Z") of impedance as a function of frequency at different temperatures (− 5 to 400 °C) for the Li_2FeSiO_4/C material

Z' decreases with an increase of frequency which shows a plateau-like behavior which demonstrates the improvement of conductivity of the material. The dispersion at low frequency is attributed to the release of interfacial polarization which in turn the migration of ions with increasing frequency and temperatures [44]. It is observed that the higher value of *Z*' at low frequency is due to polarization caused by space charge; however, its value decreases with increase in the temperatures. The results reveal that the Li_2FeSiO_4/C material obeys the negative temperature coefficient of resistance (NTCR) [45] behavior due to the semiconducting nature of the sample. It is also noticed that the *Z*' value gradually decreases with increase in the frequency hence improves ac conductivity of the material.

Figure 7c, d shows the imaginary part (*Z*") of impedance as the function of frequency at different temperatures (75 to 400 °C) for Li_2FeSiO_4/C material. It is noticed that the *Z*" decreases with increase in the frequency at low-temperature range between − 5 and 30 °C which is due to the presence of mobile species (electrons/ions) and/or immobile species. Further increasing the temperature from 50 to 275 °C, the *Z*" increases gradually and attain a maximum value due to the presence of vacancies/defects and exhibits broad peaks. The peak position shifted to a higher frequency for all the temperature range and width of the peak is decreased at higher temperatures, which suggests the presence of temperature-dependent electrical relaxation process [36] in the sample. The temperature-dependent electrical performance is not more prominent at the temperature from 150 to 200 °C. It should be noted that the peak broadening has vanished at a higher temperature and it shows frequency-independent plateau (Fig. 7d (j, k, l). The relaxation process of Li_2FeSiO_4/C material does not depend on the impedance and frequency at the measured temperature above 300 °C which indicates the presence of two different hoping mechanisms in the samples.

Arrhenius plot

The temperature-dependent conductivity of the sample has been plotted between Log (σ) and different temperatures (1000/T) are shown in Fig. 8a, b. It is noticed that the plot exhibits a slightly distorted behavior up to 15 °C which is attributed to the poor conductivity at the low-temperature region. The inference reveals that the electrical performance of the Li_2FeSiO_4/C material at low temperature (− 5 to 20 °C) is very poor which reflects in the electrochemical performance of the sample. Afterwards, (20 °C) it shows a linear region which indicates that the conductivity of the sample linearly increases with increase in the temperatures. This behavior obeys the Arrhenius model ($\sigma = \sigma_{\circ}\exp.(-Ea/kT)$) [46] which has been used to obtain the activation energy (Ea) for ionic conduction of Li_2FeSiO_4/C material. The conductivity values gradually increases with increasing in the low temperature from 15 to 50 °C. The temperature-dependent ac conductivity of the Li_2FeSiO_4/C is attributed to thermally activated process. The activation energy for ionic conduction is found to be 0.6 eV for the Li_2FeSiO_4/C material at low-temperature range (− 5 to 50 °C). The calculated activation energy for ionic transportation is 0.51 eV for Li_2FeSiO_4/C cathode materials at the temperature from 75 to 400 °C, shown in Fig. 8b. The better conductivity and activation energy at different temperatures can be attributed to the diffusion of Li-ions in different pathways and defect-mediated ionic transportations. The sample exhibits two different conduction mechanism; at low temperature, the sample possessed higher activation energy in comparison to the higher temperatures. The structure of the Li_2FeSiO_4/C involves the corner sharing of LiO_4, FeO_4, SiO_4 tetrahedrons, thus the Li-ion needs to hop much longer distances which causes the higher activation energy in the Li_2FeSiO_4/C cathode material [17]. In addition, the higher activation energy for the ionic transportation is due to the higher grain boundary resistance and structural disorder in the Li_2FeSiO_4/C material. The results reveal that the increased repulsion between LiO_4 tetrahedra and FeO_4 tetrahedra results in lower activation energy and higher electrical conductivity of the sample.

Conductivity spectra

Figure 9 shows the conductivity spectra of Li_2FeSiO_4/C material at different temperatures. The spectra show two different conduction process, frequency-independent plateau at low frequency and a dispersive region at high frequency [47]. The Li_2FeSiO_4/C at low-temperature range up to 30 °C; the frequency independent region is not the prominent flat plateau region. The frequency-independent plateau region in the material is found to be increased with the increase in temperature. The low-frequency region corresponds to the dc conductivity of the Li_2FeSiO_4/C material. The switching from frequency-independent region to frequency-dependent region shows an onset conductivity relaxation which represents long-range hopping to short-range ionic migration. The frequency-independent plateau increases with increase in the temperatures, which is attributed to the long-range hoping mechanism of the thermally activated mobile ions at higher temperatures. The conductivity of the samples is found to increase with the increase in the temperatures which obey the Jonscher's universal power law ($\sigma(\omega) = \sigma_{dc} + A\,\omega_p^{n}$) [48], where ω is the hopping frequency, *n* represents the frequency exponent, and σ_{dc} is the dc conductivity of the sample. The dc conductivity of the sample has been obtained by extrapolating the conductivity spectra to the *Y*-axis which is depicted in Table 3. It is found that the hopping rate is increased with increase in the temperature. The enhanced conductivity is due to the presence of a larger number of free electrons and higher hopping rate of collision. The better conductivity of the Li_2FeSiO_4/C material is attributed to the mobile hopping on the energetically favorable tetrahedral lattice sites. The motion of surrounding ions provides activation energy for mobile Li-ions to migrate among the polycrystalline framework.

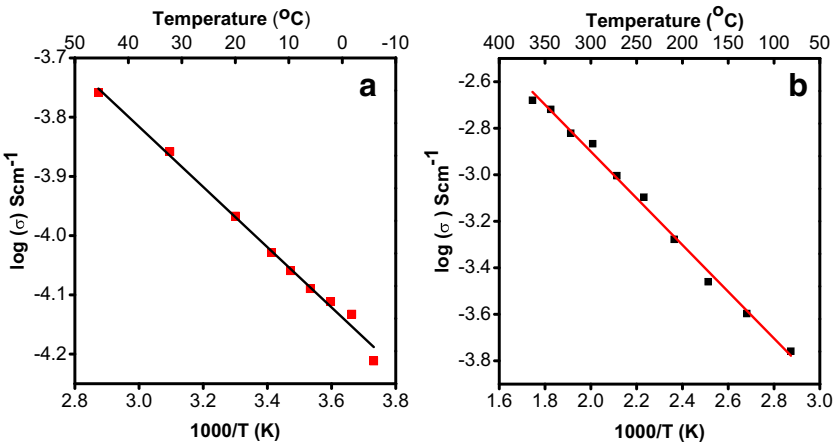

Fig. 8 The Arrhenius plot of the Li_2FeSiO_4/C cathode material, **a** temperature from − 5 to 50 °C and **b** temperature from 75 to 400 °C

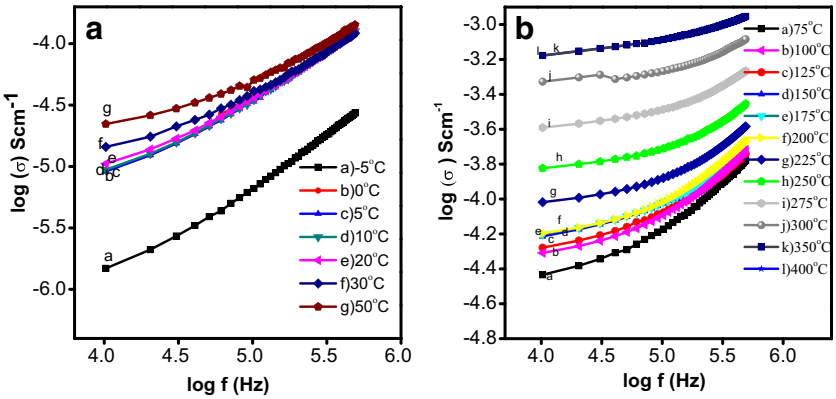

Fig. 9 **a**, **b** The variation of conductivity of the Li_2FeSiO_4/C cathode material as function of frequency at different temperatures (− 5 to 400 °C)

Electric modulus analysis

The electric modulus spectra are being used as a powerful tool to investigate the ion transport process in an ionic conductor. The electric modulus comprises the microscopic migration to macroscopic electric relaxation of the materials excluding the polarization effects [49, 50]. The relation between the impedance data and electric modulus is given below

$$M^* = M' + jM''$$
$$M' = \omega C_\circ Z' \text{ and } M'' = \omega C_\circ Z''$$

Table 3 DC conductivity of the Li_2FeSiO_4/C is calculated from conductivity spectra at different temperatures (− 5 to 400 °C)

Temperature (°C)	DC conductivity (σ_{dc}) Scm^{-1}
− 5	5.8312×10^{-7}
0	2.8532×10^{-6}
5	3.0114×10^{-6}
10	3.1296×10^{-6}
15	4.7665×10^{-6}
20	6.7639×10^{-6}
30	8.33873×10^{-6}
50	1.1558×10^{-5}
75	2.0301×10^{-5}
100	3.1455×10^{-5}
125	3.4494×10^{-5}
150	3.9667×10^{-5}
175	4.0758×10^{-5}
200	4.0331×10^{-5}
225	7.1736×10^{-5}
250	1.1339×10^{-4}
275	1.8901×10^{-4}
300	3.8770×10^{-4}
350	4.2150×10^{-4}
400	4.9980×10^{-4}

where M' and M'' are real and imaginary part of the complex modulus, geometrical capacitance $C_\circ = \varepsilon_\circ A/L$, A is the area of the material, L is the thickness of the sample, and $\varepsilon_\circ$ is the permittivity of the free space (8.854×10^{-14} F/cm). Figure 10a, b shows the real part (M') as a function of frequency at different temperatures. In the M' vs log (f) plot (Fig. 10a(a–h)), initially M' approaches to zero for all the low temperatures (− 5 to 50 °C); however, small dispersion is observed in the intermediate frequency (up to log (f): 4 Hz) which indicates the appearance of electrode polarization at low temperatures. Figure 10b(a–l) shows frequency dependence of M' for all the temperatures (75 to 400 °C), in which low frequency approaches zero suggesting elimination of electrode polarization. At higher frequency region, the M' is found to be higher for all the temperatures demonstrating the relaxation process which is attributed to the short-range mobility of charge carriers. It is observed that there is no sudden changes observed in M' vs log (f) plots and a gradual variation of M' represents the electrical relaxation process over a range of frequencies. Figure 10c, d shows the frequency dependence of M'' for the Li_2FeSiO_4/C at different temperatures. The sample does not show any Lorentzian type curves which exhibit a peak at the relaxation frequency with long tail extending to lower frequency region of short relaxation time. The peak position can be assigned to the re-orientation relaxation process of the mobile Li-ions [51]. The position of the peak in the modulus spectra shifts to higher frequency which is due to the thermally activated conduction mechanism. The shape and position of the relaxation peak depends on the conductivity in the sample which varies with frequency. The low-frequency side of the M'' indicates the range of frequencies in which charge carriers can move over a long distance and the high frequency represents localized motion. The region where peak occur indicates transition from long-range to short-range mobility with increase in frequency. This behavior (non-Debye type) suggests that the relaxation process is thermally activated in which hopping of charge carriers with small polarons is

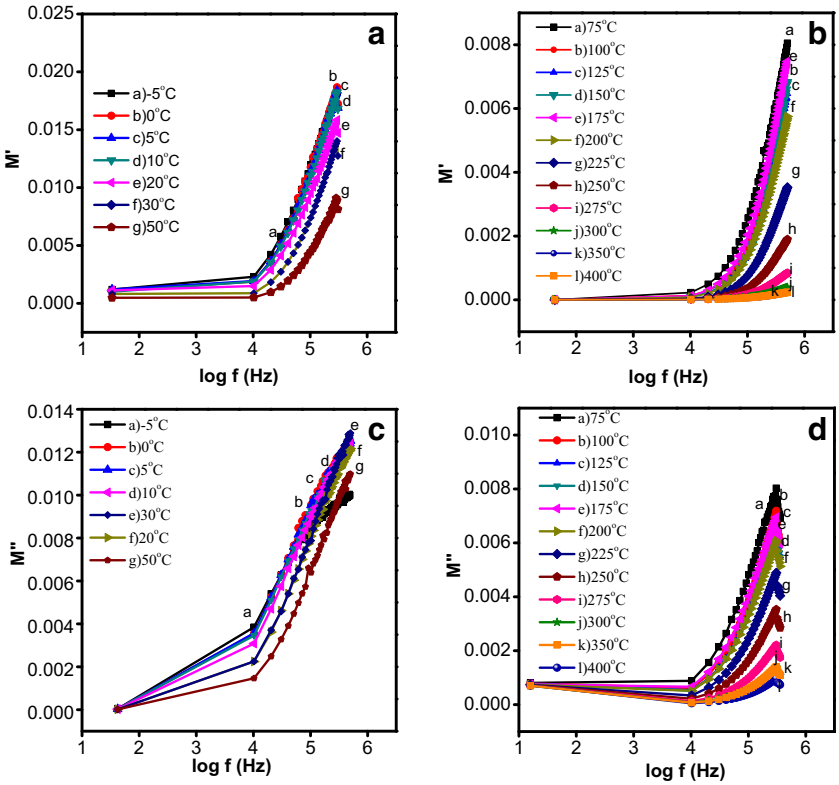

Fig. 10 **a**, **b** Real part of *M*' as a function of frequency and **c**, **d** imaginary part of *M*" as a function of frequency at different temperatures (− 5 to 400 °C) for the Li_2FeSiO_4/C material

dominated intrinsically. At higher frequency, the grain boundary movement is faster than that of low frequency which results in significant difference at high frequency.

Dielectric studies

Figure 11a–d shows the frequency dependence of dielectric functions (ε' and ε") at different temperatures for the Li_2FeSiO_4/C nano cathode material. The variation in the dielectric constant is the clear indication of polarization due to the transportation of mobile ions, electronic polarization, and lattice vibrations [52]. The complex permittivity is given below

$$\varepsilon_r = \varepsilon' + j\varepsilon''$$

where ε' is the real part of the complex permittivity or dielectric constant and ε" is the dielectric loss during each cycle of an electric field. The frequency dependence of the real part of dielectric constant ε' at different temperatures is shown in Fig. 11a, b. It is observed that the dielectric constant is found to be maximum at lower frequency regime and gradually decreases with increasing frequency for all the measured temperatures. The ε' values increase with increasing temperature from − 5 to 400 °C for all the frequency; however, the value of ε' is far higher at low frequency in comparison to the high-frequency range. Polarization mainly depends on the ability of the dipoles to orient themselves in the direction of the applied electric field. The larger value of ε' at lower frequency can be attributed to the larger time taken for dipoles to orient themselves in the direction of AC field. The presence of polarization effects at higher temperature can raise the dielectric constant [53, 54].

The dielectric loss ε" vs log (*f*) plots at different temperatures for the Li_2FeSiO_4/C nano cathode is shown in Fig. 11c, d. The dielectric behavior of the sample is explored by AC electric field at different temperatures. It should be noted that the dielectric loss is very high at low frequency which is attributed to the free charge migration in the Li_2FeSiO_4/C material. When applying the electric field to a material, the ions/electrons are reached to grain boundary by hopping from one site to another; if the grain boundary resistance is very high, the ions pile up at grain boundaries and produces the space charge polarization [55]. The absences of a peak in the dielectric loss ε" vs log (*f*) plots demonstrate the long-range ionic conduction dominance in dielectric behavior at the lower frequency for all the temperatures [56]. The variation in the dielectric loss spectra is attributed to the space charge accumulation at lower frequencies.

The dielectric loss is very high at low-frequency region, which is due to the accumulation of free ions/electrons at the interface between Li_2FeSiO_4/C material and contact electrodes. The ε' and ε" are not much prominent for the temperature range 0 to 20 °C, while these values increases with increases in the temperature up to 125 °C. The dielectric constant and loss factors does not exhibit much variation at

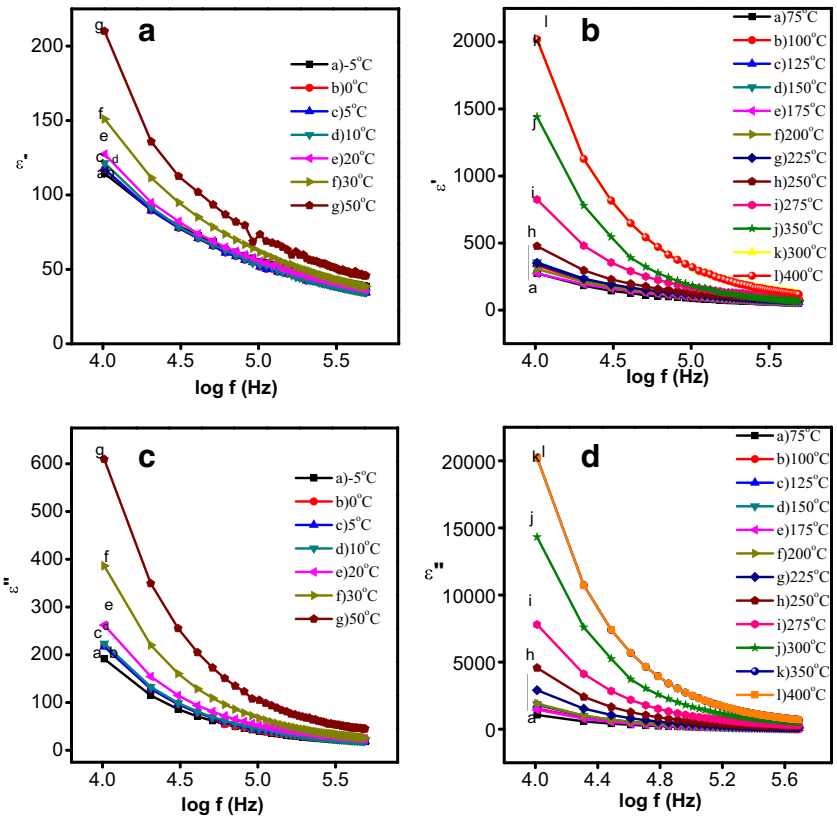

Fig. 11 **a**, **b** Dielectric constant ε' as a function of frequency and **c**, **d** dielectric loss ε" as a function of frequency at different temperatures (− 5 to 400 °C) for the Li_2FeSiO_4/C material

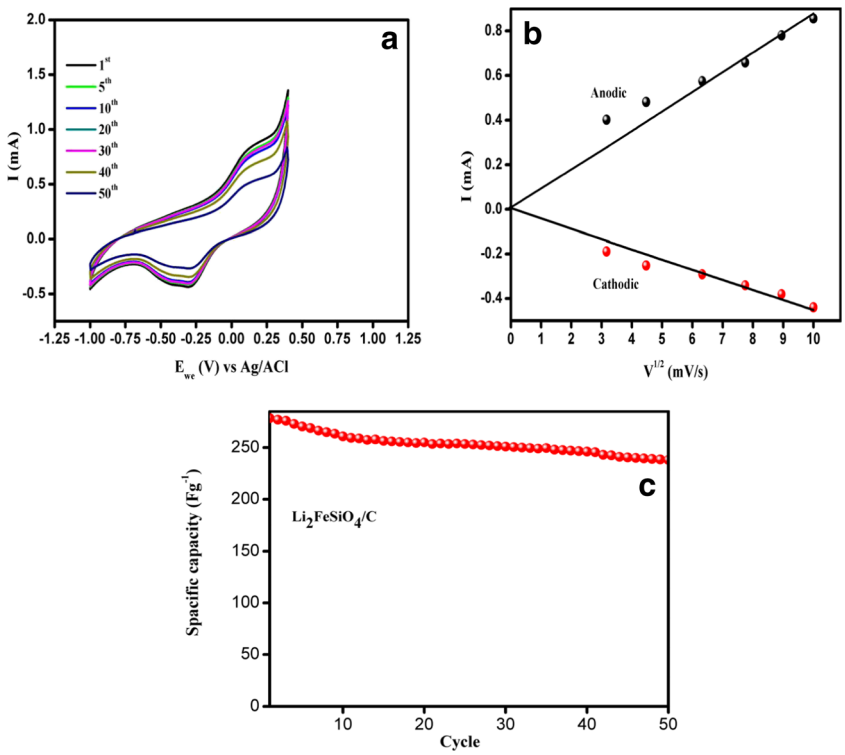

Fig. 12 **a** Cyclic voltammetric curves (scan rate is 100 mV/s), **b** the linear relationship between i_p vs $V^{1/2}$, and **c** specific capacity of the Li_2FeSiO_4 cathode material

intermediate temperature (150 to 200 °C) which might be attributed to the severe volume expansion caused by the temperature and structural re-orientation of the Li_2FeSiO_4/C sample. Further, the gradual increase of ε' and ε" with temperature can be attributed to the thermally activated defects/deformational loss and increase in the grain size that occurs in the sample at elevated temperatures.

Electrochemical characterization

Cyclic voltammetry

The redox activity of Li_2FeSiO_4/C has been tested in an aqueous-based electrochemical system at elevated temperature. The cyclic voltammetry (CV) analysis is performed in order to estimate the kinetic and mass transport during the redox process of the material. Figure 12a shows the CV curves of Li_2FeSiO_4/C cathode material over 50 cycles at a scan rate of 100 mV/s. A pair of redox peak is noticed with peak separation potential of 0.504 V. The potential difference between oxidation and reduction peaks is the promising factor for evaluating reversibility of the electrochemical reaction in a battery. The anodic peak is due to the oxidation of Fe ions by the intercalation of Li-ions from Li_2FeSiO_4/C cathode material and the cathodic peak is attributed to the reduction of Fe ions by the de-intercalation of Li-ions into the host matrix. The Li_2FeSiO_4/C cathode material displays good redox kinetics which is due to the well crystalline single phase of the Li_2FeSiO_4/C material. In addition to that, the sample delivers similar CV curves even after the 50th cycles, which may be due to the electrochemically stable orthorhombic structure with the space group of $Pmn2_1$. In the present findings, the orthorhombic structure with the space group of $Pmn2_1$ sample possesses the good cycling stability in the aqueous-based electrolyte system at room temperature. It is observed that the ratio of cathodic and anodic peak current (i_{pc}/i_{pa}) of the Li_2FeSiO_4/C is found to be 0.765 which is the indication of highly reversible nature of the material.

CV measurements at varied scan rates are used to estimate the Li-ion diffusion coefficient of the Li_2FeSiO_4/C sample. The diffusion coefficient of electrode active species of the Li_2FeSiO_4/C can be calculated by Randles-Sevcik equation [53, 57] which has been used to explore the impact of scan rates on peak current i_p. The linear plots of i_p vs $v^{1/2}$ provide the evidence for chemically reverse redox process[58]. Figure 12b display the plots of i_p as a function of $v^{1/2}$ for the Li_2FeSiO_4/C at the room temperature and good linear relationship between i_p and $v^{1/2}$ is noticed. The diffusion coefficient of the Li_2FeSiO_4/C is found to be 6.23×10^{-12} cm^2 s^{-1}. In the present work, the electrochemical performance of the Li_2FeSiO_4/C nano cathode has been examined in the aqueous-based electrolyte systems in order to explore the reversibility of the material. The primary testing reveals that the Li_2FeSiO_4/C cathode material exhibits an excellent specific capacity of 241 Fg^{-1} with good cycling stability (Fig. 12c). In addition to that, the cathode material has delivered an excellent electrical conductivity at the elevated temperature range from 50 to 125 °C, which can be optimized as optimal operating temperature for the Li_2FeSiO_4/C-based all solid-state LIBs. The temperature-dependent electrochemical performance of the Li_2FeSiO_4/C cathode material is under investigation.

Conclusion

The Li_2FeSiO_4 nano cathode material has been prepared by sol-gel method. The effect of temperature (− 5 to 400 °C) on the electrical properties of Li_2FeSiO_4/C has been explored. The XRD analysis revealed that the Li_2FeSiO_4/C possesses an orthorhombic structure with $Pmn2_1$ space group. The surface carbon coating has been substantiated from the TEM analysis of the prepared samples. The XPS and EDX analysis points out the single-phase formation of the prepared Li_2FeSiO_4/C. The bulk conductivity of the Li_2FeSiO_4 sample is found to be 1.022×10^{-4} Scm^{-1} at room temperature, which increases with an increase in temperature. The activation energy for ionic transportation is estimated to be 0.51 eV for the Li_2FeSiO_4/C material. The better electrical conductivity of the Li_2FeSiO_4/C is due to the mobile hopping on the energetically favorable tetrahedral lattice sites. The dielectric loss can be attributed to the thermally activated defects/deformational loss and increased grain size. The Li_2FeSiO_4 cathode material delivers an excellent electrochemical performance in the aqueous-based electrolyte battery system. The sample displays the similar CV curves even after the 50th cycle, which demonstrate the good cycling stability. The Li_2FeSiO_4/C nano cathode possessed excellent electrical properties at the elevated temperatures (50 to 125 °C) which can be optimized to perform the stable operation of lithium-ion batteries.

Acknowledgements Mr. P. Sivaraj thanks the Council of Scientific Industrial Research (CSIR), Govt. of India, New Delhi, for providing the necessary financial support through the Senior Research Fellowship (SRF) for the present work.

References

1. Devaraj S, Kuezma M, Ng CT, Balaya P (2013) Sol–gel derived nanostructured Li_2 $MnSiO_4$/C cathode with high storage capacity. Electrochim Acta 102:290–298
2. Armand M, Tarascon JM (2008) Building better batteries. Nature 451:652–657
3. Islam MS, Dominko R, Masquelier C et al (2011) Silicate cathodes for lithium batteries: alternatives to phosphates. J Mater Chem 27: 9811–9818

4. Armstrong AR, Kuganathan N, Islam MS, Bruce PG (2011) Structure and Lithium transport pathways in Li_2FeSiO_4 cathodes for lithium batteries. J Am Chem Soc 133:13031–13035
5. Hu L, Yang J, Amiinu IS, Kang X, Zhang W, Mu S (2015) Lithium storage properties of in-situ synthesized Li_2FeSiO_4 and $LiFeBO_3$ nanocomposites as advanced cathode materials for Lithium ion batteries. J Mater Chem A 3:23368–23375
6. Kokalj A, Dominko R, Mali G, Meden A, Gaberscek M, Jamnik J (2007) Beyond one-electron reaction in li cathode materials: designing $Li_2Mn_xFe_{1-x}SiO_4$. Chem Mater 19:3633–3640
7. Huang X, Li X, Wang H, Pan Z, Qu M, Yu Z (2010) Synthesis and electrochemical performance of Li_2FeSiO_4/C as cathode material for lithium batteries. Solid State Ionics 181:1451–1455
8. Muraliganth T, Stroukoff KR, Manthiram A (2010) Microwave-solvothermal synthesis of nanostructured Li_2MSiO_4/C (M= Mn and Fe) cathodes for lithium-ion batteries. Chem Mater 22:5754–5761
9. Zhang S, Deng C, Fu BL, Yang SY, Ma L (2010) Effects of Cr doping on the electrochemical properties of Li_2FeSiO_4 cathode material for lithium-ion batteries. Electrochim Acta 55:8482–8489
10. Yanga J, Zhenga J, Kang X et al (2016) Tuning structural stability and lithium-storage properties by d-orbital hybridization substitution in full tetrahedron Li_2FeSiO_4 nanocrystal. Nano Energy 20:117–125
11. Feng X, Fang M, He X, Ouyang M, Lu L, Wang H, Zhang M (2014) Thermal runaway features of large format prismatic lithium ion battery using extended volume accelerating rate calorimetry. J power source 255:294–301
12. Williard N, We H, Hendricks C (2013) Lessons learned from the 787 Dreamliner issue on Lithium-ion battery reliability. Energies 6:4682–4695
13. Gabrish H, Ozawa Y, Yazami R (2006) Crystal structure studies of thermally aged $LiCoO_2$ and $LiMn_2O_4$ cathodes. Electrochem Acta 52:1499–1506
14. Van Schalkwijik W, Sacrosati B (2002) Advances in lithium-ion batteries introduction, springer, N Y 47–68
15. Ramadas P, Haran B, White R et al (2002) Capacity fade of Sony 18650 cells cycled at elevated temperatures: part I. Cycling performance. J Power Sources 112:606–613
16. Nyten A, Abouimrane A, Armand M et al (2005) Electrochemical performance of Li_2FeSiO_4 as a new li-battery cathode material. Electrochemical Communication 7:156–160
17. Tana R, Yanga J, Zhenga J et al (2016) Fast rechargeable all-solid-state lithium-ion batteries with high capacity based on nano-sized Li_2FeSiO_4 cathode by tuning temperature. Nano Energy 16:112–121
18. Liua L, Wang P, Li J et al (2018) Hydrothermal preparation and intrinsic transport properties of nanoscale Li_2FeSiO_4. Solid State Ionics 320:353–359
19. Girish HN, Shao Q (2015) Advances in high capacity $LiMSiO_4$(M=Fe, Mn, Co, Ni..) cathode material for lithium ion batteries. RSC Adv 5:98666–98686
20. Sivaraj P, Nalini B, Abhilash KP, Lakshmi D, Christopher Selvin P, Balraju P (2018) Study on the influences of calcination temperature on structure and its electrochemical performance of Li_2FeSiO_4/C nano cathode for Lithium ion batteries. J Alloys Compd 740:1116–1124
21. Lu X, Chiu H-C, Kirk H et al (2016) Density functional theory insights into the structural stability and Li diffusion properties of monoclinic and orthorhombic Li_2FeSiO_4 cathodes. J Power Sources 318:136–145
22. Zaghib K, Ait Salah A, Ravet N, Mauger A, Gendron F, Julien CM (2006) Structural, magnetic and electrochemical properties of lithium iron orthosilicates. J Power Sources 160:1381–1386
23. Singh S, Mitra S (2014) Improved electrochemical activity of nanostructured Li_2FeSiO_4/MWCNTs composite cathode. Electrochim Acta 123:378–386
24. Deng C, Zhang S, Gao Y et al (2011) Regeneration and characterization of air-exposed 4 Li_2FeSiO_4. Electrochemica Acta 56:7327–7333
25. Xiao D, Shao L, Ma R et al (2013) Hydrothermal preparation of iron-based Orthosilicate cathode materials with different SiO_2 particles and their electrochemical properties. J Electrochem Sci 8:7581–7590
26. Zheng Z, Liu X, Wang L, Wu Y, Zhao H, Chen B, Xiong W (2015) Fabrication and characterization of carbon-coated Li_2FeSiO_4 nanoparticles reinforced by carbon nanotubes as high performance cathode materials for lithium-ion batteries. Electrochim Acta 168:8–15
27. Yang J, Hu L, Zheng J, He D, Tian L, Mu S, Pan F (2015) Li2FeSiO4 nanorods bonded with graphene for high performance batteries. J Mater Chem A 3:9601–9608
28. Doeff MM, James D, Wilcox RY, Aumentado A et al (2008) Impact of carbon structure and morphology on the electrochemical performance of $LiFePO_4$/C composites. J Solid State Electrochem 12:995–1001
29. Yan Z, Cai S, Miao L, Xing Z, Zhao Y (2012) Synthesis and characterization of in situ carbon-coated Li_2FeSiO_4 cathode materials for lithium ion battery. J Alloys Compd 511:101–106
30. Yang J, Kang X, He D, Zheng A, Pan M, Mu S (2015) Graphene activated 3D-hierarchical flower-like Li2FeSiO4 for high-performance lithium-ion batteries. J Mater Chem A 3:16567–16573
31. Deng C, Zhang S, Gao Y, Wu B, Ma L, Sun YH, Fu BL, Wu Q, Liu FL (2011) Regeneration and characterization of air-exposed Li_2FeSiO_4. Electrochim Acta 56:7327–7333
32. Zheng Z, Liu X, Wang L, Wu Y, Zhao H, Chen B (2015) Synthesis of Li_2FeSiO_4/C nanocomposite via a hydrothermal-assisted sol–gel process. Solid State Ionics 276:33–39
33. Itagaki M, Kobari N, Yotsuda S, Watanabe K, Kinoshita S, Ue M (2005) $LiCoO_2$ electrode/electrolyte interface of Li-ion rechargeable batteries investigated by in situ electrochemical impedance spectroscopy. J. Power Sources 148:78–84
34. Sen S, Choudhary RNP, Pramanik P (2007) Structural and electrical properties of Ca^{2+} modified PZT electroceramics. Physica B 387:56–62
35. Behera B, Nayak P, Choudhary RNP (2007) Impedance spectroscopy study of $NaBa_2V_5O_{15}$ ceramic. J Alloys Compd 436:226–232
36. Hemalatha KS, Sriprakash G, Ambika Prasad MVN, Damle R, Rukmani K (2015) Temperature dependent dielectric and conductivity studies of polyvinyl alcohol-ZnO nanocomposite films by impedance spectroscopy. Appl Phys 118:154103
37. Parameswaran AK, CS Paneerselvam, Balakrishnan N et al (2018) Electrochemical analysis of the carbon-encapsulated lithium iron phosphate nanochains and their high-temperature conductivity profiles. ACS Omega 3(6):6446–6455
38. Andre D, Meiler M, Steiner K (2011) Characterization of high-power lithium ion batteries by electrochemical impedance spectroscopy experimental investigation. J Power Sources 196:5334–5534
39. Chung SY, Bloking JT, Chiang YM (2002) Electronically conductive phospho-olivines as lithium storage electrodes. Nat Mater 1:123–128
40. Rhouma FIH, Dhahri A, Dhahri J, Valente MA (2012) Dielectric, modulus and impedance analysis of lead-free ceramics $Ba_{0.8}La_{0.133}Ti_{1-x}$ Sn $_x$ O_3 (x=0.15 and 0.2). Applied physics A 108:593–600
41. Delacourt C, Poizot P, Tarascon J-M, Masquelier C (2005) The existence of a temperature-driven solid solution in Li_xFePO_4 for $0 \leq x \leq 1$. Nat Mater 4:254–260
42. Zhou F, Marianetti CA, Cococcioni M, Morgan D, Ceder G (2004) Phase separation in LixFePO4 induced by correlation effects.

Physics Review B 69:201101. https://doi.org/10.1103/PhysRevB.69.201101
43. Zhou F, Cococcioni M, Marianetti CA, Morgan D, Ceder G (2004) First-principles prediction of redox potentials in transition-metal compounds with LDA+U. Physics Review B 70:235121
44. Gopukumar S, Jeong Y, Kim KB (2003) Synthesis and electrochemical performance of tetravalent doped $LiCoO_2$ in lithium rechargeable cells. Solid State Ionics 159:223–232
45. Rougier A, Nazri GA, Julien C (1997) Vibrational spectroscopy and electrochemical properties of $LiNi_{0.7}Co_{0.3}O_2$ cathode material for rechargeable lithium batteries. Ionics 3:170–176
46. Jha PA, Jha PK, Jha AK, Dwivedi RK (2013) Dielectric behavior of $(1-\boldsymbol{x})$ Ba $Zr_{0.025}Ti_{0.975}O_3$–$(\boldsymbol{x})$ $BiFeO_3$ solid solutions. Mater Res Bull 48:101–105
47. Senthilkumar B, KalaiSelvan R, Vinothbabu P et al (2011) Structural, magnetic, electrical and electrochemical properties of $NiFe_2O_4$ synthesized by the molten salt technique. Mater Chem Phys 130:285–292
48. Sharmila S, Janarthanan B, Chandrasekaran J (2016) Structural and electrical properties of Li_4 $Mn_{4.9}Ni_{0.1}O_{12}$ as a cathode material for rechargeable Li-ion batteries. J Appl Phys 8(1):52–58
49. Stramare S, Thangadurai V, Weppner W (2003) Lithium lanthanum titanates: a review. Chem Mater 15(21):3974–3990
50. Ngai KL, Leon C (1999) Recent advances in relating macroscopic electrical relaxation data to microscopic movements of the ions in ionically conducting materials. Solid State Ionics 125:81–90
51. Nageswara Rao B, Venkateswarlu M, Satyanarayana N (2014) Synthesis, structural and electrical properties of $Li_{1.2}Mn_{0.\ 54}Ni_{0.\ 13}Co_{0.\ 13}O_2$ synthesised by sol–gel method. Ionics 20:175–181
52. Ding Y, Zhang P, Long Z, Xu F (2009) Morphology and electrochemical properties of Al doped $LiNi_{1/3}Co_{1/3}$ $Mn_{1/3}O_2$ nanofibers prepared by electrospinning. J Alloys Compd 487:507–510
53. Ben Bechir M, Ben Rhaiem A, Bull GK (2014) Influences of sintering temperatures and crystallite sizes on electrochemical properties of $LiNiPO_4$ as cathode materials via sol–gel route for lithium ion batteries. Mater Sci 37:1–8
54. Abhilash KP, Christopher Selvin P, Nalini B, Somasundaram K, Sivaraj P, Chandra Bose A (2016) Study of the temperature dependent transport properties in nanocrystalline lithium lanthanum titanate for lithium ion batteries. J Phys Chem Solids 91:114–121
55. Murali N, Margarette SJ, Rao VK et al (2017) Structural, impedance, dielectric and modulus analysis of LiNi1-x-y-0.02Mg0.02CoxZnyO2 cathode materials for lithium-ion batteries. Journal of Science: Advanced Materials and Devices. 1–12
56. Bohnke O, Emery J, Fourquet JL (2003) Anomalies in li^+ ion dynamics observed by impedance spectroscopy and 7 Li NMR in the perovskite fast ion conductor (Li_{3x} $La_{2/3-x\square\ 1/3-2x}$) TiO_3. Solid State Ionics 158:119–132
57. Yu YW, Fietzek C, Weydanz W, Donoue K, Inoue T, Kurokawa H, Fujitani S (2007) Study of $LiFePO_4$ by cyclic voltammetry. J Electrochem Soc 154:253–257
58. Sathiyamoorthi R, Shakkthivel P, Ramalakshmi S, Shul YG (2007) Influence of mg doping on the performance of $LiNiO_2$ matrix ceramic nanoparticles in high-voltage lithium-ion cells. J Power Sources 171:922–927